NONLINEAR-AVERAGING ERRORS IN RADIATION PYROMETRY

by Donald R. Buchele

Lewis Research Center
Cleveland, Ohio

NONLINEAR-AVERAGING ERRORS IN RADIATION PYROMETRY

By Donald R. Buchele

Lewis Research Center
Cleveland, Ohio

NATIONAL AERONAUTICS AND SPACE ADMINISTRATION

NONLINEAR-AVERAGING ERRORS IN RADIATION PYROMETRY

by Donald R. Buchele

Lewis Research Center

SUMMARY

The error in measuring the average of a fluctuating temperature by optical means is determined for cases of temporal or spatial fluctuation with small optical depth. The method is applicable to line-reversal, absorption-emission, and other pyrometric methods that involve the measurement of the absolute or relative magnitudes of radiant flux. It is also applicable to some techniques of gas analysis by radiometric means. Experimental confirmation of the analysis is described for a Gaussian probability density distribution.

The analysis accounts for a previously reported discrepancy of a few percent between a line-reversal pyrometer and other types of local (probe-type) pyrometers.

INTRODUCTION

The accuracy of optical methods of measuring gas temperature is often impaired when time or space variations in gas temperature affect the amount of radiant flux delivered to the instrument. Since radiated flux is an exponential function of temperature, the result is a nonlinear averaging of temperature as determined by flux measurement.

Some experimental conditions (illustrated in fig. 1) that may lead to errors in temperature measurement are the following:

(a) Constant emissivity throughout the line of sight (fig. 1(a)). Gas flow is observed by an optical system over a path length L and a cross section MP. (Symbols are defined in appendix A.) The radiated flux Φ from a gas of high emissivity ($\epsilon_\lambda \approx 1.0$) and large optical depth $k_\lambda L$ originates mainly from one end of the optical path. For a gas of low emissivity ($\epsilon_\lambda \ll 1.0$) all parts contribute equally.

(b) Variations of absorption coefficient along the line of sight and with wavelength (fig. 1(b)). Within the finite wavelength interval accepted by the flux detector, $k_\lambda L$ may vary from zero to a value much greater than unity; this is typically the case for spectral line radiation. Some of the optical methods (ref. 1) require constant emissivity over the wavelength interval of measurement.

The absorption coefficient is shown also as varying with L. This may be the result of a temperature profile that changes the composition of the gas, or the result of a radiating material added locally to the gas stream. Local addition of sodium from a movable probe was used in the investigations of references 2 and 3 to obtain a temperature profile by the line-reversal method. This avoided the error of averaging a profile.
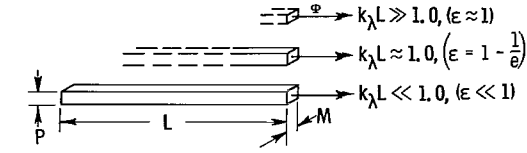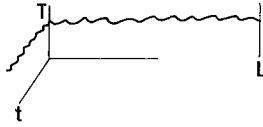

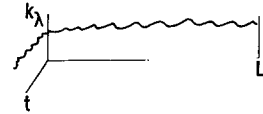(a) Radiated flux weighted by emissivity.
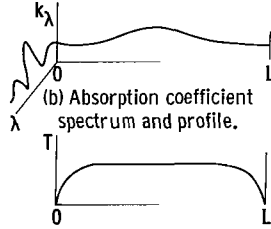
(b) Absorption coefficient spectrum and profile.

(c) Temperature profile.

(d) Fluctuating temperature.

(e) Fluctuating absorption coefficient.

Figure 1. - Experimental conditions.

(c) Temperature profile along the line of sight (fig. 1(c)). A temperature profile may exist along the line of sight as in the cross section of flow from a nozzle. The radiated flux depends on the absorption coefficient distribution (figs. 1(a) and (b)). A temperature profile can also exist in the directions M and P (fig. 1(a)). The combined effect of temperature profile and absorption coefficient is reported in reference 4.

(d) Time variation in temperature (fig. 1(d)). A fluctuating temperature may be caused by imperfect combustion. The fluctuation may be in time for a flowing gas, or in space along lengths L, M, and P for either a stationary or a flowing gas. Fluctuation measurements are given in reference 5.

(e) Time variation in absorption coefficient (fig. 1(e)). Often a variation in absorption coefficient will accompany variation in temperature. For example, the change is substantial for a concentration of the hydroxyl molecule in flame gases.

For a combination of conditions (c) and (d), in which a local temperature $T(x,t)$ varies with time and location, and of conditions (b) and (e), in which a local gas absorption coefficient varies with time and with wavelength $(k_\lambda = k_\lambda(x,t,\lambda))$, the resultant local radiance is $N_\lambda = N_\lambda(x,t,\lambda)$. The apparent average radiance $\overline{N}_g$ of the gas is

$$\overline{N}_g = \frac{1}{t_1} \int_0^\infty \int_0^L \int_0^{t_1} N_\lambda k_\lambda e^{-\int_x^L k_\lambda \, dx} \, dt \, dx \, d\lambda \qquad (1)$$

where the exponential factor is the radiant transmittance from a local point in the gas to the gas boundary, and t_1 is the time interval over which the measurement is averaged. In practice, the equation must be simplified by approximations appropriate to the experiment. The following are examples of such simplifications:

(1) A narrow-band filter may limit the wavelength interval so that all quantities may be assigned monochromatic values.

(2) The absorption coefficient may be so low that the exponential factor may be assumed to be unity.

(3) The absorption coefficient may be assumed constant.

(4) The fluctuation amplitude may be assumed nearly constant from 0 to L.

(5) The temperature profile may be flat enough so that it may be assumed to contribute negligible error.

In the subsequent analysis of temperature fluctuations, approximations (1), (2), and (5) will be used. These approximations simplify equation (1) so that it becomes

$$\overline{N}_{\lambda,g} = \frac{1}{t_1} \int_0^L \int_0^{t_1} N_\lambda k_\lambda \, dt \, dx \tag{2}$$

To integrate equation (2) in terms of temperature, it is necessary to substitute $N_\lambda(T)$ for N_λ given by Wien's radiation equation, $k_\lambda = k_\lambda(T)$ depending on the partial pressure of the radiating molecule, and then substitute some function $T(x,t)$. If, at any x, the temperature $T_x(t)$ is fluctuating only slightly about a mean value $\overline{T}$, it is not necessary to have the explicit function $T_x(t)$. It is sufficient to use the probability density distribution $p(T_x)$ of the temporal fluctuations of temperature about the mean value $\overline{T}$. Therefore, the average given by equation (2) may be replaced by an average in terms of $p(T_x)$ as

$$\overline{N}_{\lambda,g} = \int_0^L \int_{-\infty}^{\infty} N_\lambda(T) k_\lambda(T) p(T_x) dT \, dx \tag{3}$$

The quantity $\overline{N}_{\lambda,g}$ is the average of the means $\overline{N}_{\lambda,g,x}$ at any x along the optical path L, where

$$\overline{N}_{\lambda,g,x} = \int_{-\infty}^{\infty} N_\lambda(T) k_\lambda(T) p(T_x) dT \tag{4}$$

Since a Gaussian distribution of temperature about an average value (Gaussian probability density function) is often approached in experiments, this distribution will be assumed. Experimental evidence will be presented later to show that this assumption was valid in a representative test facility burning gasoline and air.

The dependence of the averaging error on other functional forms of the distribution is treated in appendix B. The cases treated will be those in which temperature varies periodically with time.

ANALYSIS

In a gas of thermal temperature T, the spectral radiance is given by the Wien equation as

$$N_\lambda = c_1 \lambda^{-5} e^{-c_2/\lambda T} \tag{5}$$

The Wien equation deviates from the exact Planck equation by less than 1 percent for $\lambda T < 3000$ $(\mu)(^\circ K)$, and less than 10 percent for $\lambda T < 6000$ $(\mu)(^\circ K)$.

The absorption coefficient k_λ for one constituent of a gas mixture is proportional to the partial pressure, which in turn is proportional to the equilibrium constant of the gas mixture when the partial pressure is a small fraction of the gas pressure. In turn, the equilibrium constant varies exponentially with temperature according to the van't Hoff thermodynamic equation, so that

$$k_\lambda = A e^{-B/T} \tag{6}$$

where A and B are constants, and B can be determined by using values of partial pressure as a function of temperature computed by the method of reference 6. Thus, equations (5) and (6) may be combined to yield

$$N_\lambda k_\lambda = A c_1 \lambda^{-5} e^{-\frac{1}{T}\left(\frac{c_2}{\lambda} + B\right)} \tag{7}$$

For a Gaussian distribution about an average temperature $\overline{T}$

$$p(T) = \frac{1}{\pi \, \Delta T} e^{-\left[(T-\overline{T})/\sqrt{\pi} \, \Delta T\right]^2} \tag{8}$$

where ΔT is the average deviation of the fluctuations, and by definition,

$$\int_{-\infty}^{\infty} p(T) dT \equiv 1$$

Substituting equations (7) and (8) into equation (4) yields

$$\bar{N}_{\lambda,g} = \frac{Ac_1\lambda^{-5}}{\pi\,\Delta T}\int_{-\infty}^{\infty} e^{-\frac{1}{T}\left(\frac{c_2}{\lambda}+B\right)-\left(\frac{T-\bar{T}}{\sqrt{\pi}\,\Delta T}\right)^2}\,dT \tag{9}$$

As $T - \bar{T}$ becomes large, the exponent of e becomes a large number. Consequently, the term containing $1/T$ may be approximated by a parabola. A parabola that matches $1/T$ at $\bar{T}$ and has the same slope there in terms of the variable $T - \bar{T}$ is

$$\frac{1}{T} = \frac{1}{\bar{T}} - \frac{T-\bar{T}}{\bar{T}^2} + \frac{C(T-\bar{T})^2}{\bar{T}^3} \tag{10}$$

where a constant C will be determined.

Integration after completing the square in the exponent yields

$$\bar{N}_{\lambda,g,x} = \frac{Ac_1\lambda^{-5}}{\sqrt{1+C\gamma}}\,e^{-\frac{1}{\bar{T}}\left(\frac{c_2}{\lambda}+B\right)\left[1-\frac{\gamma}{4(1+C\gamma)}\right]} \tag{11}$$

where

$$\gamma = \left(\frac{c_2}{\lambda}+B\right)\frac{\pi}{\bar{T}}\left(\frac{\Delta T}{\bar{T}}\right)^2 \tag{12}$$

The average optically determined thermal temperature $\bar{T}_o$ is defined by

$$\bar{N}_{\lambda,g,x} = k_\lambda c_1\lambda^{-5}\,e^{-c_2/\lambda\bar{T}_o} \tag{13}$$

The averaging error $\bar{T}_o - \bar{T}$ is obtained from equations (11) and (13) as

$$\bar{T}_o - \bar{T} = \bar{T}\left(\frac{1}{\beta}-1\right) \tag{14}$$

5

where

$$\beta = 1 - \frac{\gamma}{4(1 + C\gamma)} + \frac{\overline{T} \ln(1 + C\gamma)}{2\left(\dfrac{c_2}{\lambda} + B\right)} \tag{15}$$

Figure 2 is a plot of equation (14) for constant values of $c_2/\lambda\overline{T}$ and a constant C equal to 0.8. This value of the constant yields an averaging error within 5 percent of that obtained by numerical integration of equation (9) for $\Delta T/\overline{T} < 0.15$ and $(\overline{T}_0 - \overline{T})/\overline{T} < 0.1$. The values of $(c_2/\lambda + B)/\overline{T}$ in figure 2 are for the indicated wavelengths radiated by hydroxyl (OH) and water (H_2O) molecules and sodium (Na) atoms at $1800°$ K with $B = 0$ for Na and H_2O and $B = 18,600°$ K for OH.
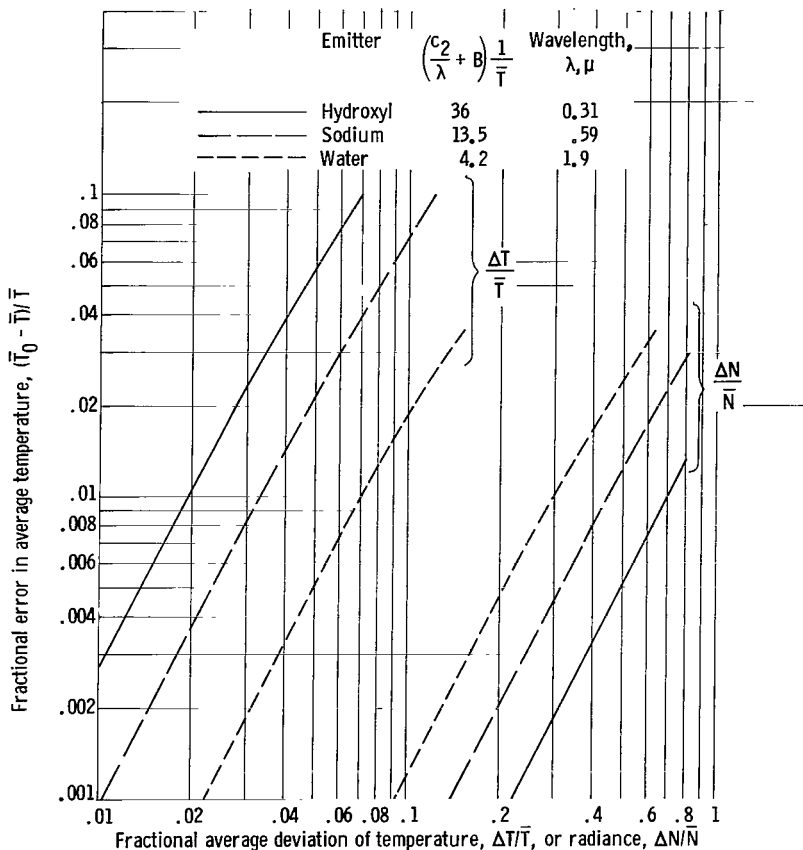

Figure 2. - Average-temperature error due to Gaussian probability density distribution. Average temperature, $1800°$ K.

The average optically determined temperature $\overline{T}_0$ may be measured by sodium-line reversal. Average deviation ΔT may be measured electrically with an alternating current meter that responds to the average value of fluctuations in the detector output voltage. For such radiant-flux measurement, equation (7) is differentiated, and the result is

$$\Delta T = \frac{\overline{T}^2}{\dfrac{c_2}{\lambda} + B} \frac{\Delta(N_\lambda k_\lambda)}{\overline{N}_\lambda k_\lambda} \tag{16}$$

where $\overline{N}_\lambda k_\lambda$ is proportional to the detector output average (direct-current) voltage, and $\Delta(N_\lambda k_\lambda)$ is proportional to the detector output average deviation (alternating current) voltage. Substituting equation (16) into equation (12) yields the averaging error $(\overline{T}_0 - \overline{T})/\overline{T}$ in terms of radiance fluctuation. This is plotted in figure 2. The radiance measurement is subject to attenuation by space-averaging of $\Delta(N_\lambda k_\lambda)$ along the optical path, unless a probe-type of sensor is used. Selection of a long wavelength for this measurement minimizes an error caused by the nonlinear relation between N_λ and T in equation (7).

In the course of development of a radiometer-pyrometer, the instrument was tested by being used to measure temperature in a gasoline-burning jet (ref. 7). The exhaust gas flowed through a concentric ASME nozzle that produced a jet of 3-inch diameter. Since low-temperature combustion products in the optical path outside the jet would absorb water radiation, this absorption was minimized by using an air purge in a tube that extended up to the jet boundary (fig. 3(a)).
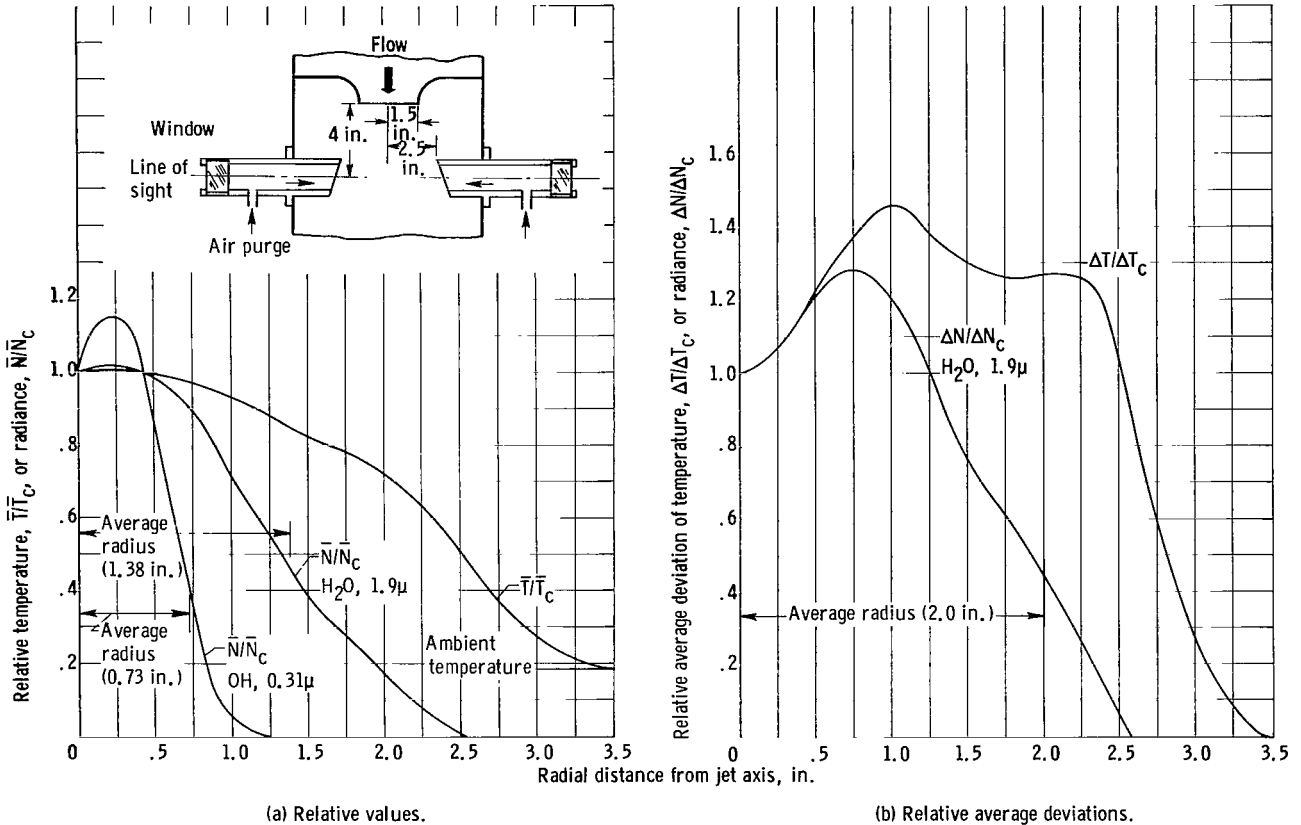

(a) Relative values.

(b) Relative average deviations.

Figure 3. – Profiles of temperature and calculated radiance. Average temperature, 1800° K.

Temperature fluctuations were measured with a bare-wire crossflow thermocouple of 0.01-inch diameter (ref. 8) and with the radiometer, which used the 1.9-micron emission from water vapor in the combustion products. Frequency response of the thermocouple was extended to 65 cps by a transformer-type compensator (ref. 9). Frequency response of the radiometer was limited by its amplifier to 600 cps. The average deviation of the signal fluctuation was measured with the vacuum tube voltmeter for both the radiometer and the thermocouple.

The average temperature was measured with a self-balancing potentiometer for the thermocouple. The average radiance was measured with a vacuum-tube voltmeter for the radiometer by means of chopped radiation. The voltmeter was of the type that measures the average value of an alternating-current waveform,

with a low-frequency response to 1 cps. The signal with chopped radiation was a square wave with a peak-to-peak amplitude equal to the radiated flux. This amplitude was twice the voltmeter reading for an ideal square wave. A temperature profile taken with the thermocouple is shown in figure 3(a). Corresponding calculated radiance profiles are shown for OH and H_2O at specified wavelengths, with an optical depth much less than 1.0. The temperature profile was converted to radiance by using equation (7) at 1.9 microns for H_2O, and at 0.31 micron for OH radiation with $B = 0$ for H_2O and $B = 18,600°$ K for OH. An average radius of the gas jet is indicated, which, when multiplied by the radiance at the jet axis, would yield the same flux as that produced by the actual profile.

A temperature fluctuation profile taken with a thermocouple is shown in figure 3(b). The corresponding calculated radiance fluctuation profile is shown for H_2O at the specified wavelength, with an optical depth much less than 1.0. An average radius of the gas jet is indicated, which, when multiplied by the average deviation at the jet axis, would yield the same alternating flux as that produced by the actual profile.

The following table gives the percent average deviation of gas temperature $\Delta T/\overline{T}$ from 1800° K as measured by the thermocouple on the jet axis and by the radiometer averaging across the jet: The radiometer average deviation of 1.4 percent on the jet axis was estimated to be the ratio of the average radius for water of figure 3(a) to the average radius of figure 3(b) multiplied by the radiometer measured value. The smaller average deviation shown by the radiometer on the jet axis may be attributed to the attenuation caused by optical space-averaging across the gas stream.

Measuring device	Frequency bandwidth, cps		
	1 to 65		1 to 600
	On jet axis	Average over optical path	
	Average temperature deviation, percent		
Thermocouple	3.2	---	[a]4.0
Radiometer[b]	[a]1.4	2.0	2.5

[a]Estimated.
[b]With water at 1.9 μ.

The existence of attenuation due to optical space-averaging was demonstrated by making measurements with two thermocouples initially placed side by side near the jet axis. Their frequency response was extended to 22 cps by a resistance-capacitance compensator (ref. 9). Their outputs were recorded with a double-beam oscillograph as one thermocouple was moved radially from the jet axis while the other remained fixed on the axis. The close agreement of the two waveforms (fig. 4(a)) quickly vanished at greater distances (figs. 4(b), (c), and (d)). The two thermocouple outputs were also fed to a correlator to give the correlation coefficient plotted in figure 5. An average distance l is indicated, which,

(a) 1/8 Inch from jet axis. (b) 1/2 Inch from jet axis. (c) 1 Inch from jet axis. (d) $1\frac{1}{2}$ Inches from jet axis.
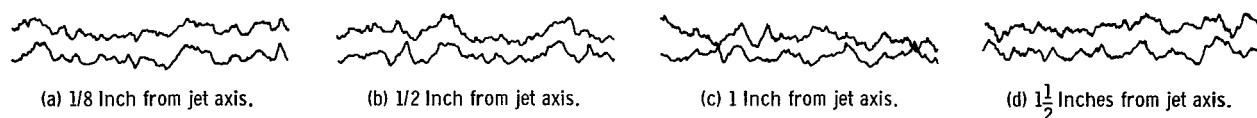
Figure 4. – Oscillograph records of thermocouple signal amplitudes at axial and several radial positions. (Lower trace on jet axis.)

when multiplied by a coefficient of 1.0, would yield the same area as that under the curve. The distance l is approximately 1/2 inch, whereas the jet diameter $2R$ of figure 3(b) is 4 inches. Since l is small compared with this diameter, as an approximatio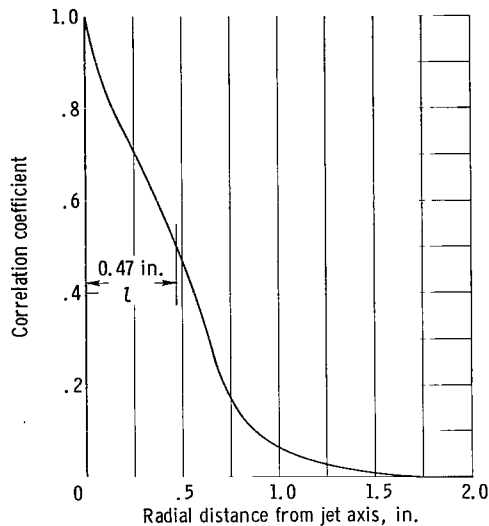n the gas lying along the optical path can be replaced by a fictitious distribution consisting of four zones of length $2l$, each of which may be treated as radiating independently of the others and radiating an equal amount of flux. The average fluctuation from all four zones will be $\sqrt{4}$ times the fluctuation of any one zone, whereas the average flux will be four times that radiated from one zone. Therefore, the fluctuation of 1.4 percent given by the radiometer on the jet axis (previous table) should appear as a local fluctuation of 2.8 percent after correction for attentuation due to space-averaging. This conclusion agrees quite well with the value of 3.2 percent recorded by the thermocouple.

Figure 5. - Correlation curve for thermocouple at jet axis.

These experiments thus clearly indicate the existence of attenuation due to both time-averaging and space-averaging. They indicate also that the average deviation of the fluctuations, as might be deduced from an oscilloscope record of radiometer output, would be smaller than the true average deviation because of attenuation by space-averaging. In the particular
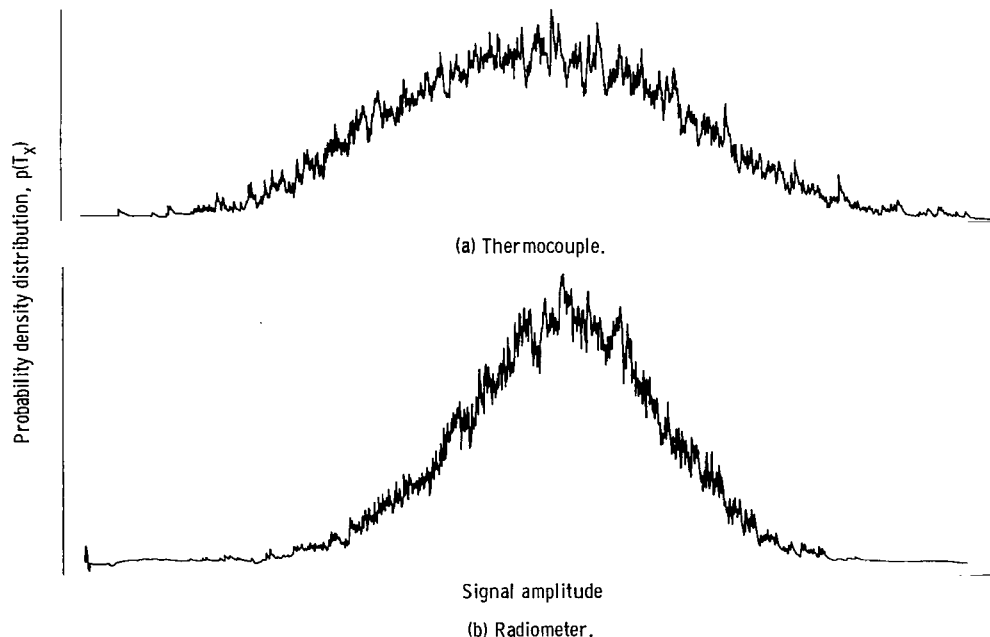

(a) Thermocouple.

(b) Radiometer.

Figure 6. - Measured probability density distribution of signal amplitude.

experimental apparatus used here, the attenuation by space-averaging was of the same order of magnitude as the time-averaging attentuation.

The frequency content of the fluctuations is predominantly less then 600 cps, because a tenfold increase of the radiometer from 65 to 600 cps corresponds to only a 25 percent increase in average deviation (table on p. 8).

The increase from 2.0 to 2.5 shown in the table on page 8 for the radiometer at the 600-cps frequency limit would also be expected for a thermocouple that had the same frequency response. Thus, the most likely percentage fluctuation of the gas temperature would be 4 percent for a probe-type sensor with a frequency response of up to 600 cps. The corresponding error of a sodium-line reversal temperature measurement is 1.45 percent, based on figure 2. A correction of this amount would account for the discrepancy at 1800° K between the line-reversal method and the other temperature probes reported in reference 7.

The probability density distribution of amplitude fluctuations was recorded by an analyzer described in reference 10. The temperature distribution obtained with the thermocouple is shown in figure 6(a), and the radiance distribution obtained with the radiometer is given by figure 6(b). Both distributions are of the Gaussian shape that was assumed in deducing the correction method. The same results were obtained at other distances from the jet axis. The oscillograph records of amplitude, given in figure 4 (p. 8), illustrate the random waveforms.

CONCLUSION

Because of the nonlinear relation between radiance and temperature, the average radiance measured corresponds to a temperature higher than the average temperature. It was found that the error in the average of a fluctuating temperature

(1) Increases with the square of the average deviation of fluctuation

(2) Varies inversely with wavelength, being greater at shorter wavelengths

(3) Approaches the average deviation at wavelengths in the visible spectrum as the average deviation increases and approaches 10 percent

(4) Is relatively independent of the functional form of the probability density distribution of temperature

These conclusions apply when the temperature is averaged over some period of integration. In addition, attenuation by space-averaging of the temperature fluctuations over the optical path may contribute an additional error.

In a test facility designed for smooth combustion of gasoline and air, a Gaussian probability density distribution of temperature was recorded. The corresponding temperature error by the sodium line-reversal measurement was 1.5 percent.

Lewis Research Center
    National Aeronautics and Space Administration
        Cleveland, Ohio, May 21, 1964

APPENDIX A

SYMBOLS

A,B   parameters of van't Hoff eq. (6)

C   constant of parabola eq. (10); $C = 0.8$

c_1, c_2 Planck radiation constants; $c_2 = 1.438$ (cm)($^{\circ}$K)

E   constant defined following eq. (B1)

F   rectangular wave parameter defined by eq. (B4)

K_1, K_2 constants of eq. (B7)

k_λ spectral absorption coefficient

L   path length, in.

l distance between thermocouples, in.

M   width of optical path, in.

N   radiance, w/(steradian)(cm^2)

$\overline{N}_g$ average radiance of gas

N_λ spectral radiance, w/(steradian)(cm^3)

P   height of optical path, in.

$p(T_x)$ probability density distribution

R   radius of jet, in.

T   temperature, $^{\circ}$K

$\overline{T}$ average temperature, $^{\circ}$K

T_F temperature greater than average, $^{\circ}$K

T_G temperature less than average, $^{\circ}$K

$\overline{T}_o$ average optically determined temperature, $^{\circ}$K

t   time, sec

x   distance along optical path, in.

β parameter defined by eq. (14)

γ parameter defined by eq. (12)

ϵ_λ spectral emissivity

λ wavelength, cm

Φ radiated flux, w

Subscript:

c   on centerline of jet

Superscript:

$(\overline{})$ average

AVERAGING ERROR WITH PERIODIC WAVEFORMS

For the distributions considered here, $p(T)$ is an algebraic function. The integration makes use of the Taylor series expansion of the Wien radiation equation itself instead of an expansion of the exponent of the Wien equation as was used in the section ANALYSIS. The expansion is

$$e^{-E/T} = e^{-E/\overline{T}}\left[1 + \frac{E}{\overline{T}}\frac{T-\overline{T}}{\overline{T}} + \frac{1}{2}\left(\frac{E^2}{\overline{T}^2} - \frac{2E}{\overline{T}}\right)\left(\frac{T-\overline{T}}{\overline{T}}\right)^2 + \frac{1}{6}\left(\frac{E^3}{\overline{T}^3} - \frac{6E^2}{\overline{T}^2} + \frac{6E}{\overline{T}}\right)\left(\frac{T-\overline{T}}{\overline{T}}\right)^3 \right.$$

$$\left. + \frac{1}{24}\left(\frac{E^4}{\overline{T}^4} - \frac{12E^3}{\overline{T}^3} + \frac{36E^2}{\overline{T}^2} - \frac{24E}{\overline{T}}\right)\left(\frac{T-\overline{T}}{\overline{T}}\right)^4 + \cdots\right] \tag{B1}$$

where

$$E = \frac{c_2}{\lambda} + B$$

Sinusoidal Waveform

For a sinusoidal temperature fluctuation $T - \overline{T} = (\pi/2)\Delta T \sin\theta$, the distribution is

$$p(T) = \frac{1}{\pi\left[\left(\frac{\pi}{2}\Delta T\right)^2 - (T-\overline{T})^2\right]^{1/2}} \tag{B2}$$

having the limits $-\Delta T\,\pi/2 < T - \overline{T} < \Delta T\,\pi/2$. Integrating equations (B1) and (B2) and following the procedure in the section ANALYSIS give

$$\beta = 1 - \frac{\overline{T}}{E}\ln\left[1 + \frac{\pi^2}{16}\left(\frac{E^2}{\overline{T}^2} - \frac{2E}{\overline{T}}\right)\left(\frac{\Delta T}{\overline{T}}\right)^2 + \frac{\pi^4}{1024}\left(\frac{E^4}{\overline{T}^4} - \frac{12E^3}{\overline{T}^3} + \frac{36E^2}{\overline{T}^2} - \frac{24E}{\overline{T}}\right)\left(\frac{\Delta T}{\overline{T}}\right)^4 + \cdots\right]$$

$$\tag{B3}$$

Rectangular Waveform

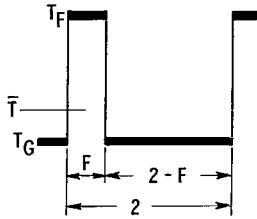The rectangular waveform shown in figure 7 has a parameter F such that $F = 1$ for a square wave. The relations are

Figure 7. - Rectangular wave-form.

$$T_F - \overline{T} = \frac{\Delta T}{F} \qquad (B4)$$

$$\overline{T} - T_G = \frac{\Delta T}{2 - F}$$

where

$$T_F > \overline{T} > T_G$$

The average radiance due to the temperatures T_F and T_G is

$$\overline{N}_\lambda = \frac{FN_{\lambda,F} + (2 - F)N_{\lambda,G}}{2} \qquad (B5)$$

Integrating equations (B1), (B4), and (B5) and following the procedure in the section ANALYSIS give

$$\beta = 1 - \frac{\overline{T}}{E} \ln\left\{1 + \frac{1}{4}\left(\frac{1}{F} + \frac{1}{2 - F}\right)\left(\frac{E^2}{\overline{T}^2} - \frac{2E}{\overline{T}}\right)\left(\frac{\Delta T}{\overline{T}}\right)^2 + \frac{1}{12}\left[\frac{1}{F^2} - \frac{1}{(2 - F)^2}\right]\left(\frac{E^3}{\overline{T}^3} - \frac{6E^2}{\overline{T}^2} + \frac{6E}{\overline{T}}\right)\left(\frac{\Delta T}{\overline{T}}\right)^3\right.$$

$$\left. + \frac{1}{48}\left[\frac{1}{F^3} - \frac{1}{(2 - F)^3}\right]\left(\frac{E^4}{\overline{T}^4} - \frac{12E^3}{\overline{T}^3} + \frac{36E^2}{\overline{T}^2} - \frac{24E}{\overline{T}}\right)\left(\frac{\Delta T}{\overline{T}}\right)^4 + \cdots\right\} \qquad (B6)$$

Small Error Approximation

For small errors, where $\Delta T/\overline{T} \ll 1$, the temperature error equations, obtained by combining equation (13) with equations (14) and (B3) or (B6), take the form

$$\frac{\overline{T}_o - \overline{T}}{\overline{T}} = K_1\left(\frac{E}{\overline{T}} - 2C\right)\left(\frac{\Delta T}{\overline{T}}\right)^2 + K_2\left(\frac{E^2}{\overline{T}^2} - \frac{6E}{\overline{T}} + 6\right)\left(\frac{\Delta T}{\overline{T}}\right)^3 \qquad (B7)$$

where E is defined by equations (B1) and (5) and the constants K_1, K_2, and C are given in the following table:

14

Temperature variation	K_1	K_2	C	Oscillograph waveform
Random (Gaussian distribution)	0.79	0	0.8	
Sinusoid	.62	0	1	
Square wave, F = 1.0	.50	0	1	
Rectangular wave				
F = 0.7	.55	.12	1	
.5	.67	.30	1	
.3	.98	.90	1	
1.7	.98	-.90	1	
1.5	.67	-.30	1	
1.3	.55	-.12	1	

This table shows that K_1 is not sensitive to the type of temperature variation. The wave shape can usually be identified with sufficient precision to estimate K_1 and K_2 by observing an oscilloscope pattern.

A numerical example of the rectangular type of temperature variation is given in the following table to indicate the relative magnitude of the two terms of equation (B7) with an asymmetrical waveform:

Waveform	Average temperature, $\overline{T}$, °K	$\Delta T/\overline{T}$	First term in eq. (B7)	Second term in eq. (B7)	$\overline{T}_o - \overline{T}$, °K Computed	$\overline{T}_o - \overline{T}$, °K Exact
0.5 cycle	2837.5	0.0224	0.0045	0	12.85	12.7
0.15 cycle	2837.5	.0224	.0089	.0029	33.5	32.8
0.85 cycle	2837.5	.0224	.0089	-.0029	17.0	18.1

REFERENCES

1. Broida, H. P.: Experimental Temperature Measurements in Flames and Hot Gases. Temperature, Its Measurement and Control in Sci. and Industry, Reinhold Pub. Corp., 1955, vol. 2, pp. 265-286.

2. Tamkin, S. J., and Arnold, G. B.: Ramjet High Temperature Determinations by the Sodium-D-Line Spectral Reversal and Gas Analysis Methods. Rep. 4-8, Univ. Southern Calif., Feb. 1, 1948.

3. Lezberg, Erwin A., and Lancashire, Richard B.: Recombination of Hydrogen-Air Combustion Products in an Exhaust Nozzle. NASA TN D-1052, 1961.

4. Strong, H. M., and Bundy, F. P.: Measurement of Temperatures in Flames of Complex Structure by Resonance Line Radiation, pts. I-III. Jour. Appl. Phys., vol. 25, no. 12, Dec. 1954, pp. 1521-1537.

5. Tourin, R. H.: Monochromatic Radiation Pyrometry of Hot Gases, Plasmas, and Detonations. Temperature, Its Measurement and Control in Sci. and Industry, vol. 3, pt. II, Reinhold Pub. Corp., 1962, pp. 455-466.

6. Zeleznik, Frank J., and Gordon, Sanford: A General IBM 704 or 7090 Computer Program for Computation of Chemical Equilibrium Compositions, Rocket Performance, and Chapman-Jouget Detonations. NASA TN D-1454, 1962.

7. Glawe, G. E., Johnson, R. C., and Krause, L. N.: Intercomparison of Several Pyrometers in a High-Temperature Gas Stream. Temperature, Its Measurement and Control in Sci. and Industry, vol. 3, pt. II, Reinhold Pub. Corp., 1962, pp. 601-605.

8. Scadron, M. D., Warshawsky, I., and Gettleman, C. C.: Thermocouples for Jet-Engine Gas Temperature Measurement. I.S.A. Proc., vol. 7, 1952, p. 142.

9. Shepard, C., and Warshawsky, I.: Electrical Techniques for Time Lag Compensation of Thermocouples Used in Jet Engine Gas Temperature Measurements. Instruments, vol. 26, no. 11, Nov. 1953, pp. 1725-1730.

10. Carlson, E. R., Conger, C. C., Laurence, J. C., Meyn, E. H., and Yocke, R. A.: Special Electronic Equipment for the Analysis of Statistical Data. Proc. IRE, vol. 47, no. 5, pt. I, May 1959, pp. 956-962.

"The aeronautical and space activities of the United States shall be conducted so as to contribute . . . to the expansion of human knowledge of phenomena in the atmosphere and space. The Administration shall provide for the widest practicable and appropriate dissemination of information concerning its activities and the results thereof."

—NATIONAL AERONAUTICS AND SPACE ACT OF 1958

NASA SCIENTIFIC AND TECHNICAL PUBLICATIONS

TECHNICAL REPORTS: Scientific and technical information considered important, complete, and a lasting contribution to existing knowledge.

TECHNICAL NOTES: Information less broad in scope but nevertheless of importance as a contribution to existing knowledge.

TECHNICAL MEMORANDUMS: Information receiving limited distribution because of preliminary data, security classification, or other reasons.

CONTRACTOR REPORTS: Technical information generated in connection with a NASA contract or grant and released under NASA auspices.

TECHNICAL TRANSLATIONS: Information published in a foreign language considered to merit NASA distribution in English.

TECHNICAL REPRINTS: Information derived from NASA activities and initially published in the form of journal articles.

SPECIAL PUBLICATIONS: Information derived from or of value to NASA activities but not necessarily reporting the results of individual NASA-programmed scientific efforts. Publications include conference proceedings, monographs, data compilations, handbooks, sourcebooks, and special bibliographies.

Details on the availability of these publications may be obtained from:

SCIENTIFIC AND TECHNICAL INFORMATION DIVISION

NATIONAL AERONAUTICS AND SPACE ADMINISTRATION

Washington, D.C. 20546